Structure and Dynamics of Pyramidic Liquid Crystals by Deuterium NMR and X-ray Diffraction

R. Poupko,[†] Z. Luz,*[,†] N. Spielberg,[‡] and H. Zimmermann[§]

Contribution from The Weizmann Institute of Science, Rehovot 76100, Israel, Department of Physics, Kent State University, Kent, Ohio 44242, and Max-Planck-Institut für medizinische Forschung, D-6900 Heidelberg, West Germany. *Received October 31, 1988*

Abstract: Pyramidic liquid crystals are mesogens derived from the cone-shaped tribenzocyclononene (TBCN) core, substituted with appropriate side chains. The pyramidic mesophases consist of two-dimensional columnar structures in which the rigid cores of the mesogen molecules are stacked in parallel on top of each other. In the present work X-ray and deuterium NMR measurements on the solid and mesomorphic phases of homologues of the alkyloxy (I-*n*) and alkanoyloxy series (II-*n*) are reported. In the P_A mesophase of series I-*n*, the columns form a two-dimensional hexagonal array with a single molecule per unit cell. Deuterium NMR measurements on three specifically deuterated isotopomers of I-8 (including species deuterated at the unsubstituted aromatic sites, crown-ring methylenes and α-methylene of the side chain) indicate that within this mesophase two types of uncorrelated motions with very different correlation times can be distinguished: (i) fast fluctuations of the molecular C_3 axis, which results in an effective orientational order of $S = 0.85$, essentially independent of temperature; (ii) planar reorientation about the C_3 axis. The rate of the latter process is within the dynamic range of deuterium NMR, allowing its determination by line-shape analysis. Assuming this motion to correspond to planar diffusion, a diffusion constant at room temperature of $D_R(300\ K) = 6.8 \times 10^5$ rad^2/s with an activation energy of $\Delta E = 63$ kJ/mol is derived from the experimental spectra. At least the first three atoms in the alkyloxy side chains do not participate in fast (on the NMR time scale) conformational isomerization in the solid or in the P_A mesophase. The high-temperature mesophase of series II-*n*, P_C, is very similar to the P_A mesophase of I-*n*. It has an hexagonal structure with, however, four columns per unit cell. Deuterium line-shape analysis on specifically deuterated II-13 species indicates the same type of averaging motions as in the P_A mesophase with an orientational order parameter of $S = 0.93$ (independent of temperature), and $D_R(373\ K) = 1.4 \times 10^5$ rad^2/s with $\Delta E = 112$ kJ/mol. The low-temperature mesophase of this series, P_D, is biaxial and appears to be rectangular or very nearly so. It is much less mobile than the P_C mesophase, as evidenced by lack of planar reorientation, although there are still fast fluctuations of the molecular C_3 axis (giving $S = 0.93$). Unlike in the alkyloxy (I-*n*) series, in the alkanoyloxy (II-*n*) series there is fast side-chain isomerization in the P_C and P_D mesophases and to some extent even in the solid. The line shape of the α-methylene deuterons in the P_D mesophase suggest a two-site jump process, while in the high-temperature P_C phase, additional motions appear to set in, resulting in further narrowing of the spectrum width. Additional deuterium NMR measurements on deuterated I-8, II-11, and II-13 dissolved in nematic solvents in order to determine molecular structural parameters are reported.

Several new types of thermotropic liquid crystalline mesophases were recently discovered. Among these, the so-called pyramidic or bowlic[1-8] mesophases occupy a unique place because of the special structure of the corresponding mesogen molecules. The pyramidic mesogens consist of a tribenzocyclononene (TBCN) core to which flexible side chains are linked via ether or ester bonds. So far four homologue series of TBCN were shown to be mesogenic:

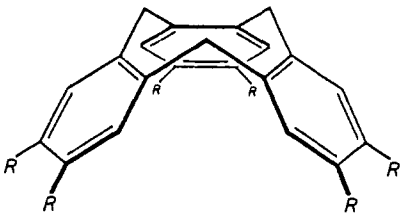

(I) R = $C_nH_{2n+1}O$–
(II) R = $C_{n-1}H_{2n-1}C(O)O$–
(III) R = $C_{n-1}H_{2n-1}OC_6H_4C(O)O$–
(IV) R = $C_{n-1}H_{2n-1}C_6H_4C(O)O$–

Some of their structural characteristics were already studied by optical microscopy and X-ray diffraction techniques.[1-5] It was shown that series I compounds with *n* ranging between 6 and 12 exhibit a single uniaxial mesophase, P_A. Series II compounds are mesogenic for $n \geq 8$, exhibiting a single biaxial mesophase, P_D, for $8 \leq n < 11$, while the homologues with $11 \leq n \leq 14$ possess two mesophases: P_D, at low temperatures and an hexagonal mesophase, P_C, at higher temperatures. Above 14 carbons per side chain the homologues exhibit only the P_C mesophase. All mesophases were shown by optical microscopy to consist of columns which are believed to be formed by stacked mesogen molecules. Since these molecules lack a plane of symmetry perpendicular to their symmetry axis, they are most likely stacked parallel to each other forming columns with a macroscopic electric dipole and consequently may form mesophases with special electric properties.[1] It is therefore of special interest to investigate their structural and dynamic properties on a molecular level. X-ray measurements on two members of series II ($n = 10, 12$) and one member of series III were previously reported.[4] These studies confirmed the columnar structure and symmetries of P_C and P_D as determined by the optical microscopy observations, and provided information on the dimensions of the corresponding unit cells.

In the present work we extend the X-ray studies to yet another member of series II (II-13), and to three members of series I (I-8, I-9, and I-10). We also performed extensive deuterium NMR measurements on several isotopomers of two homologues belonging respectively to series I-*n* and II-*n*, viz., I-8 and II-13. These measurements provide detailed information on the dynamic state of the molecules, particularly with regard to the reorientation of the mesogen molecules about their C_3 axis, as well as about their orientation order in the various mesophases. It turns out that in the P_A mesophase of I-*n* and the P_C mesophase of II-*n*, the reorientation rate falls within the dynamic deuterium NMR range, thus allowing accurate kinetic measurements of the reorientation

[†] The Weizmann Institute of Science.
[‡] Kent State University.
[§] Max-Planck-Institut für medizinische Forschung.

(1) Zimmermann, H.; Poupko, R.; Luz, Z.; Billard, J. *Z. Naturforsch.* **1985**, *40a*, 149.
(2) Zimmermann, H.; Poupko, R.; Luz, Z.; Billard, J. *Z. Naturforsch.* **1986**, *41a*, 1137.
(3) Malthête, J.; Collet, A. *Nouv. J. Chim.* **1985**, *9*, 151.
(4) Levelut, A. M.; Malthête, J.; Collet, A. *J. Phys.* **1986**, *47*, 357.
(5) Malthête, J.; Levelut, A. M.; Tinh, N. H. *J. Phys. Lett.* **1985**, *46*, L-875.
(6) Lin Lei *Wuli* **1982**, *11*, 171; *Mol. Cryst. Liq. Cryst.* **1987**, *146*, 41. Leung, K. M.; Lin Lei *Mol. Cryst. Liq. Cryst.* **1987**, *146*, 71.
(7) Collet, A. *Tetrahedron* **1987**, *43*, 5725.
(8) Malthête, J.; Collet, A. *J. Am. Chem. Soc.* **1987**, *109*, 7544.

0002-7863/89/1511-6094$01.50/0

process to be made. The computational procedures used for analyzing the dynamic line shapes are outlined in the Appendix.

Experimental Section

Synthesis. The isotopically normal mesogens of series I-*n* and II-*n* were synthesized as described previously.[1] For the NMR measurements three different specifically deuterated species of each of the I-8 and II-13 homologues were prepared. They include isotopomers deuterated in (i) the unsubstituted sites of the aromatic ring, (ii) the methylene groups in the crown ring, and (iii) the α-methylene of the side chains. They were synthesized from appropriately labeled hexahydroxytribenzocyclononene by esterification with tridecanoyl chloride, or by alkylation with octyl bromide.

Deuterated hexahydroxytribenzocyclononene was obtained by cleavage of the corresponding hexamethoxytribenzocyclononene (cycloveratrylene) with boron tribromide: 5 g of cycloveratrylene was dissolved in 250 mL of dry chloroform, and 13 mL of BBr_3 was added dropwise at room temperature. The mixture was refluxed overnight and evaporated; the dry residue was crystallized from water/ethanol, yielding 4 g of the desired intermediate product.

Cycloveratrylene was synthesized from paraformaldehyde and 1,2-dimethoxybenzene (veratrole). In a typical reaction 13 g of paraformaldehyde and 50 g of veratrole were stirred in 400 mL of HCl (37%), first at room temperature for 3 h and then at 60 °C for 5 h more. After cooling, the crystalline solid was collected over a glass filter, dried for several days in the air, and repeatedly crystallized from benzene (yielding 13 g of cycloveratrylene × 1 mol of benzene).

To obtain crown-ring deuterated cycloveratrylene the above procedure was used with deuterated paraformaldehyde, while for cycloveratrylene deuterated in the aromatic rings, 1,2-dimethoxybenzene-*3,4,5,6-d*$_4$ and concentrated DCl/D_2O were used. The deuterated veratrole was prepared by exchange: 18 g of isotopically normal veratrole was allowed to react with 200 g of D_3PO_4 (85% in D_2O) at 80 °C for 2 days. After cooling, the solution was repeatedly extracted with ether, the solvent removed, and the final product distilled. The yield was 15 g of veratrole of 96 atom % deuterium.

II-13 deuterated in the side-chain α-methylene groups was obtained by esterification with tridecanoyl-α-*d*$_2$ chloride, prepared from the corresponding acid by reaction with $SOCl_2$. Deuteration of the acid was effected by mixing 15 g of isotopically normal tridecanoic acid, 4 g of NaOH (pellets), and 100 mL of D_2O (99.8 atom %) in a high-pressure stainless steel vessel and allowing the mixture to react at 200 °C for 3 days. The α-deuterated acid (>95 atom %) was recovered by bulb–tube distillation.

The I-8 compounds were prepared by alkylation with octyl bromide as described in ref 1, except for one of the isotopomers [(I-8)^{ii}] for which a modified, more efficient alkylation procedure was used. Rather than reacting octyl bromide with hexahydroxytribenzocyclononene, the corresponding hexaacetoxytribenzocyclononene was used: 1 g of the latter compound and 8 g of octyl bromide dissolved in 40 mL of isobutyl methyl ketone containing 4 g of K_2CO_3 were refluxed under constant stirring for 6 days. The solution was then evaporated to complete dryness under reduced pressure (10^{-3} mm) for 12 h; the hexaoctyloxytribenzocyclononene was recovered (1 g) by column chromatography on silica gel (CH_2Cl_2/*n*-hexane 7:3).

The appropriately labeled hexaacetoxytribenzocyclononene was obtained from the corresponding cycloveratrylene by first cleaving the methoxy groups with BBr_3 as described above. After evaporation of the solvent the residue was dissolved in a large excess of acetic anhydride containing traces of concentrated H_2SO_4, then heated to 80 °C for 30 min. The mixture was then recooled to room temperature, poured over ice, and filtered; the precipitate was recrystallized from nitromethane/ethanol.

To prepare I-8 deuterated in the side-chain α-methylene, octyl-α-*d*$_2$ bromide was used in the alkylation process. It was prepared by reduction of octanoic acid ethyl ester with $LiAlD_4$ to octanol-*1-d*$_2$, which was converted to octyl bromide by reaction with Br_2 and red phosphorus.

In addition to the above-mentioned isotopically labeled compounds, we also describe in the text results for chain perdeuterated II-11. It was synthesized by esterification with perdeuterated undecanoyl chloride obtained from the corresponding acid with $SOCl_2$. Perdeuterated undecanoic acid was obtained by mixing 15 g of the normal acid, 4 g of NaOH (pellets), 3 g of Pt on carbon (10%) with 100 mL of D_2O (99.8 atom %) in a high-pressure stainless steel vessel and allowing the mixture to react at 160 °C for 6 days. The labeled acid was then isolated by acidification and extraction, and finally distilled. This procedure was repeated a second time. The final yield was 12 g of 95–97 atom % acid (the first step yielded 80 atom % deuteration).

Nematic Solvents. Some measurements were performed in nematic solvents, viz. phase V (consisting of mixtures of azoxy compounds) and ZLI2452 (consisting of a mixture of esters of phenyl- and biphenylcyclohexane). Both compounds were obtained from E. Merck, Darmstadt.

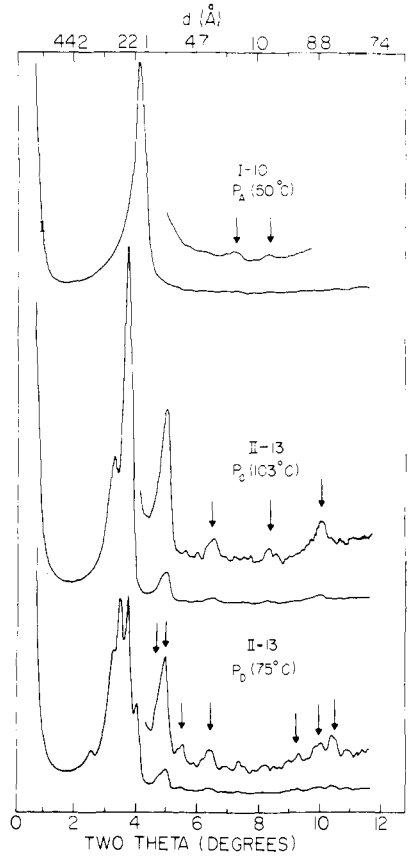

Figure 1. X-ray diffraction pattern obtained from (from top to bottom) the P_A mesophase of I-10 at 50 °C, the P_C mesophase of II-13 at 103 °C, and the P_D mesophase of II-13 at 75 °C. The arrows indicate the positions used in the final analysis of some of the weaker peaks enhanced by signal averaging.

NMR Measurements. Deuterium NMR measurements were performed at 46.1 MHz on a high-power Bruker CXP300 spectrometer, equipped with a BVT1000 variable-temperature unit. The spectra were recorded by the quadrupole echo method, with 90° pulse widths (t_p) of 2.5–3 μs. The time interval between pulses was usually 20 μs, although some experiments were done with varying τ's.

X-ray Measurements. X-ray diffraction patterns were recorded using a transmission specimen focusing powder diffractometer with a curved LiF monochromator in the incident beam and with temperature-controlled specimen stage.[9] The X-ray tube was operated at 640 W (32 kV, 20 mA). Some of the diffraction peaks of interest were very weak (in some cases, only 1 or 2 counts/s over a background of 30 counts/s) so that it was necessary to carry out repeated scans over the regions of interest. For example, for I-8, 11 scans of approximately 40-min duration each were necessary in order to measure the (11) reflection. This point is illustrated in Figure 1 which shows the diffraction intensities of this compound from a single scan. The arrows indicate the peak positions as determined by averaging over several scans.

For each diffraction peak, an experimental error was assigned, indicating the uncertainty in the location of the peak. This arises primarily from two sources: counting statistics and overlap of diffraction lines. In the latter case when a low-intensity peak is superposed on a steep shoulder of a high-intensity peak, the precise position, intensity, and width of the low-intensity peak depend on the shape assumed for the high-intensity peak.

Results and Discussion

As indicated in the Introduction X-ray and NMR measurements were performed on members of both series I-*n* and II-*n*. Accordingly, the discussion is divided into two parts corresponding to the results obtained from members of the two series.

(9) Goldfarb, D.; Luz, Z.; Spielberg, N.; Zimmermann, H. *Mol. Cryst. Liq. Cryst.* **1985**, *126*, 225.

Table I. d-Spacings and Lattice Parameters in the P_A Mesophase Region of Series I Compounds

compd	Miller indices hkl	lattice parameter[a] (Å)	d(meas) (Å)	d(calc) (Å)
I-8	10	21.75	18.80 (0.09)	18.84
	11		10.94 (0.07)	10.99
	20			9.42[b]
	(−)[c]		4.5	
I-9	10	22.53	19.50 (0.17)	19.51
	11		11.29 (0.22)	11.27
	20		9.67 (0.27)	9.76
	(−)[c]		4.5	
I-10	10	23.57	20.44 (0.12)	20.41
	11		11.71 (0.17)	11.79
	20		10.15 (0.19)	10.21
	(−)[c]		4.5	

[a] Average values over the mesophase region assuming hexagonal symmetry. (Numbers in parentheses are rms derivations from the averages.) [b] Not observed. [c] This line corresponds to the high-angle peak.

I. Hexaalkyloxytribenzocyclononene (Series I-n). A. X-ray Measurements. Three homologues of this series were investigated by X-ray, viz., I-8, I-9, and I-10. Their general phase diagram is:

$$K_1 \xrightarrow{(T_1)} P_A \xrightarrow{(T_2)} L$$

where K_1 is a crystalline solid, P_A a uniaxial mesophase, and L the isotropic liquid; T_1 = 24.9, 18.7, 25.5 °C and T_2 = 71.5, 66.1, and 63.2 °C for the n = 8, 9, and 10 homologues, respectively.[1] The X-ray diffraction pattern of these compounds in the isotropic liquid show two broad peaks, corresponding to d-spacing of 21 to 22 Å, and 4.5 to 4.6 Å. These spacings approximately fit the distances of closest approach perpendicular and parallel to the molecular C_3 axis.

The P_A mesophases in I-9 and I-10 exhibit three low-angle peaks (one strong and two very weak) and a broad signal at high angles (see upper trace in Figure 1, which corresponds to the low-angle region of I-10), while compound I-8 exhibits in addition to the broad signal only two low-angle peaks (one strong and one weak). The d-spacings are essentially independent of temperature, and their values are summarized in Table I. We have analyzed the low-angle data, on the basis of an hexagonal columnar structure, with the high-angle peak ($d \approx 4.5$ Å) corresponding to the stacking distance of the molecules within the columns. As may be seen in the table, these results correspond to lattice parameters, a, ranging from 21.75 Å for I-8 to 23.57 Å for I-10. These parameters were determined by averaging the measured d-spacings over the mesophase region, but with more weight given to the values of the strong (10) reflections. From these X-ray results and an estimated specific gravity of $\rho \approx 1$, it may be concluded that in the P_A phase there is one column per 2D unit cell.

It is instructive to compare these results with estimates of the diameters of the I-n molecules, which should at least approximately correspond to the diameter of the columns and hence to the corresponding lattice parameters. From crystallographic data for the tribenzocyclononene core,[10-12] a value of 4.87 Å is calculated for the radial distance from the molecular C_3 axis to the bridging oxygen atoms. If it is assumed that the alkyl chains are fully extended in an all-trans configuration perpendicular to C_3, an overall diameter of 34 Å is estimated for I-9, which is much larger than the observed lattice parameter of 22.5 Å. Even if the assumption is made that the chains are stretched continuously along the "edge" of the pyramid, the resulting effective molecular diameter of 28 Å is still considerably larger than the experimental lattice parameter. It must therefore be concluded that in the P_A mesophase the side chains are highly folded with perhaps some interpenetration between neighboring columns, or that they are helically twisted around the C_3 axis.[4]

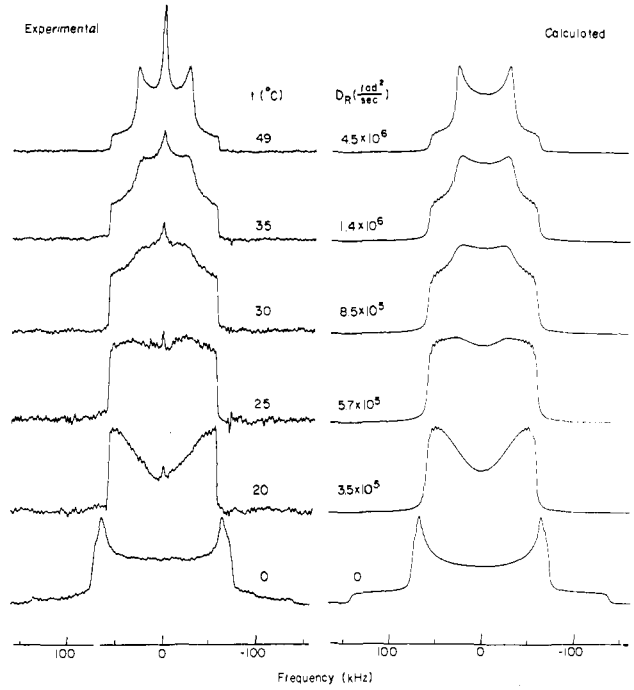

Figure 2. Deuterium NMR spectra of the aromatic deuterons of (I-8)^i in the solid (bottom traces) and P_A mesophase. The spectra on the left are experimental and were recorded on heating from the solid (except for the 20 °C trace which was obtained by supercooling) by the quadrupole echo method at the indicated temperatures (τ = 20 μs). The traces on the right are simulated and were computed from eq A16 and integration over α, using the planar diffusion constants, D_R, indicated in the figure. The lower trace which corresponds to the rigid limit was calculated using a powder pattern program. The magnetic parameters used are given in Table II.

A strictly hexagonal arrangement of the columns should result in a ferroelectric phase,[1] since antiferroelectric order cannot be fitted into a hexagonal array. We have as yet not been able to determine the dielectric properties of the pyramidic mesophases because of their high viscosity; however, it appears that a ferroelectric arrangement would have a high-energy content and that therefore an arrangement in which the columns are randomly oriented parallel and antiparallel to the director is a more plausible structure.

B. NMR Measurements. NMR measurements were made only on the I-8 homologue of the alkyloxy series. Three different isotopomers of this compound were studied: (i) deuterated in the unsubstituted aromatic sites (I-8)^i, (ii) deuterated in the crown-ring methylenes (I-8)^{ii}, and (iii) deuterated in the α-methylene of the side chains (I-8)^{iii}. Species i and ii provide information on the rigid part of the mesogen molecules, particularly with regard to its reorientational modes of motion and orientational order parameter, while species iii relates to the behavior of the side chains.

1. Aromatic Deuterons. In Figure 2 are shown deuterium NMR spectra of (I-8)^i, i.e., of the aromatic deuterons, in the solid state (bottom trace), and at several temperatures in the P_A mesophase. The spectrum of the solid is characteristic of a rigid powder in which the molecules are fixed in space and do not undergo reorientational motion. It can be simulated[13] using an effective line width $1/T_2 = 10^4$ s^{-1}, and quadrupole interaction parameters $\nu_Q = 3e^2qQ/4h$ = 135 kHz, $\eta \approx 0.06$, which fall in the characteristic range of static aromatic deuterons.[14]

Upon heating to the P_A mesophase a discontinuous change in the spectrum takes place, consisting of narrowing of the overall

(10) Cerrini, S.; Giglio, E.; Mazza, F.; Pavel, N. V. *Acta Crystallogr.* **1979**, *B35*, 2605.
(11) Hyatt, J. A.; Duesler, E. M.; Curtin, D. Y.; Paul, I. C. *J. Org. Chem.* **1981**, *45*, 5074.
(12) Collet, A.; Gabard, J.; Jacqies, J.; Cesario, M.; Guilhem, J.; Pascard, C. *J. Chem. Soc., Perkin Trans. 1* **1981**, 1630.
(13) Siderer, Y.; Luz, Z. *J. Magn. Reson.* **1980**, *37*, 449.
(14) Barnes, R. G. *Adv. Nucl. Quadrupole Reson.* **1974**, *1*, 335.

Table II. Magnetic Parameters Used in the Line Shape Analysis of the Deuterium NMR Spectra in the Various Phases of I-8 and II-13

phase	parameter	(I-8)[i]	(I-8)[ii]	(I-8)[iii]
solid	ν_Q(kHz)	135 (η = 0.06)	132	117
	$1/T_2$ (s^{-1})	10^4	10^4	10^4
P_A	$\langle\nu_Q\rangle$ (kHz)	115	113	100–94[a]
	$1/T_2$ (s^{-1})	10^4	2.0–3.5 × 10^3[b]	3.5 × 10^3
	S	0.85	0.85	0.85–0.80[a]

		(II-13)[i]	(II-13)[ii]	(II-13)[iii]
solid	ν_Q (kHz)	136	130	115
P_D	$\langle\nu_Q\rangle$ (kHz)	127	121	50 (η = 0.95)[c]
	S	0.93	0.93	
P_C	$\langle\nu_Q\rangle$ (kHz)	127	121	54 ($\eta \approx 0$);[c,d] 13 ($\eta \approx 1$)[c,d]
	S	0.93	0.93	

[a] Range of fitted values between 30 and 50 °C. [b] For D^{in}, $1/T_2 = 2 \times 10^3$ s^{-1}; for D^{ou}, $1/T_2 = 3.5 \times 10^3$ s^{-1}. [c] Average over chain isomerization. [d] These results vary somewhat with temperature.

spectral width to less than half of the solid-state spectrum, and a modified line shape which is strongly dependent on the temperature within the mesophase region. This suggests the occurrence of a dynamic process at a rate comparable to the quadrupole interaction constant. As shown below, this line shape can be fitted to a dynamic model in which the molecules undergo planar reorientational diffusion about their C_3 axis. The quantitative analysis of the results also indicates a reduction of ν_Q with respect to its value in the solid. This is most likely due to fast fluctuations (uncorrelated to the reorientation) of the columnar axis whose effect can be described in terms of an effective orientational order for the C_3 axis, $S = \langle {}^1/_2(3\cos^2\gamma - 1)\rangle$. (In this expression for S, γ is the instantaneous angle between the director and the molecular C_3 axis, and the angular brackets indicate averaging over all molecules in a domain.)

To obtain kinetic parameters for the reorientation process, we compare the experimental results with simulated spectra calculated for various rates of reorientational diffusion.[15,16] The computation procedure is described in the Appendix, where, in fact, we consider two reorientational mechanisms: the planar diffusion mentioned above and a symmetric three-site jump model.[16] The line shapes computed for the two models are, however, very similar, preventing us from distinguishing between the two mechanisms. We therefore analyze the results in terms of the planar diffusion model which seems to us more reasonable on physical grounds.

In the computation we assume that the samples consist of an isotropic distribution of domains. In order to ensure that the experiments indeed correspond to such a distribution, the spectra for the kinetic measurements were always recorded upon heating from the solid and avoiding getting too close to the clearing point, where some alignment and therefore deviation from isotropic distribution of domains sometimes took place. In the line-shape calculations the effect of the fast fluctuations of the C_3 axis is introduced by reducing the quadrupole interaction parameter from its solid-state value ν_Q to $\langle\nu_Q\rangle = S\nu_Q$ (we neglect the small effect due to nonzero η).

The simulated spectra shown in the right columns in Figure 2 were calculated so as to best fit the experimental results in the left column. The parameters used are given in the figure and in Table II. The reorientation diffusion constant, D_R, derived from the fitting of the spectra are plotted in Figure 3 versus the reciprocal absolute temperature. From this plot an activation energy, ΔE = 63 kJ/mol, and a room-temperature diffusion constant, $D_R(300\text{ K}) = 6.8 \times 10^5$ rad^2 s^{-1}, are obtained.

To ascertain the interpretation of the dynamic line shape in terms of the assumed model, and to determine more accurately the kinetic parameters, we extended the line-shape analysis to spectra recorded at various intervals, τ, between the $\pi/2$ pulses in the quadrupole echo sequence. It is well known that in the presence of a dynamic process the line shape (and intensity) of quadrupole echo spectra depends on τ and gives rise to characteristic "quadrupole echo distortions", thus providing additional means to determine the kinetic parameters of the system.[17,18] The necessary mathematical relations applicable to the present case are given in the Appendix. We have applied this procedure to the dynamic spectra of the aromatic deuterons of I-8, and an example recorded at 30 °C for τ ranging from 12 to 250 μs is shown in Figure 4. The figure also shows simulated spectra calculated for the corresponding τ values and a common set of kinetic and magnetic parameters ($D_R = 8.5 \times 10^5$ s^{-1}; $1/T_2 = 10^4$ s^{-1}; $\langle\nu_Q\rangle$ = 115 kHz). It may be seen that the fit of the spectral line shape is indeed very satisfactory.

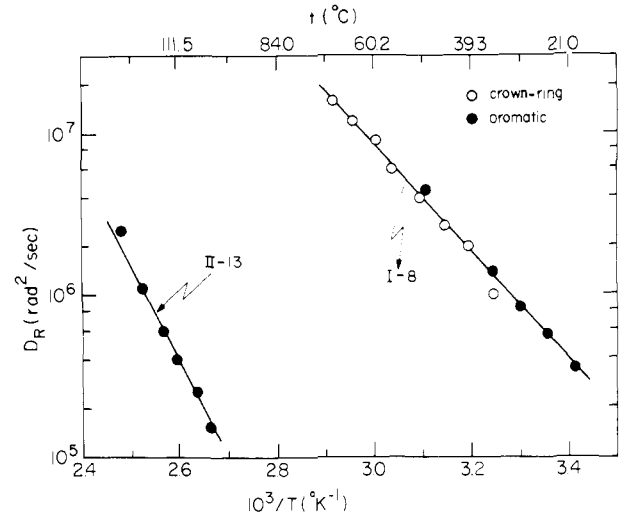

Figure 3. Arrhenius plot of the planar diffusion constant, D_R, for the P_A mesophase of I-8, derived from the aromatic and crown-ring deuterons in $(I\text{-}8)^i$ and $(I\text{-}8)^{ii}$, and for the P_C mesophase of II-13, derived from the aromatic deuterons in $(II\text{-}13)^i$.

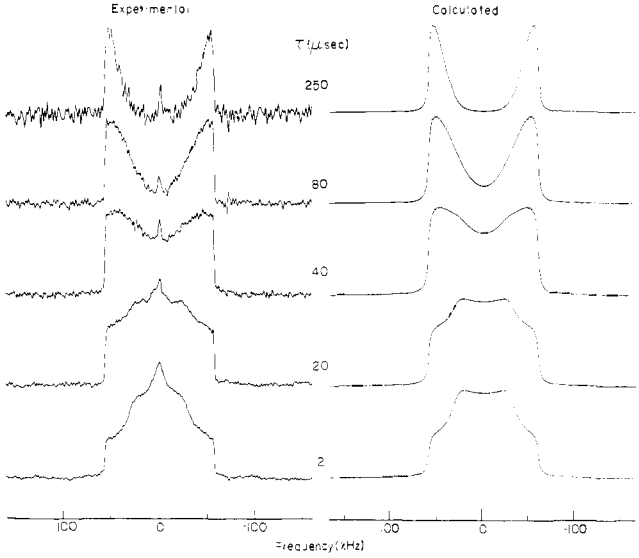

Figure 4. Dependence of the dynamic line shape of the aromatic deuterons in the P_A mesophase of $(I\text{-}8)^i$ on the time interval, τ, between the $\pi/2$ pulses in the quadrupole echo sequence. The spectra on the left are experimental (total of 4000 scans each) at 30 °C. The spectra on the right are simulated as in Figure 2 for the P_A mesophase with $D_R = 8.5 \times 10^5$ rad^2/s.

2. Crown-Ring Deuterons. In the left column of Figure 5 are depicted NMR spectra of the crown-ring deuterons of $(I\text{-}8)^{ii}$ in the solid and P_A mesophase at various temperatures. The solid-

(15) Luz, Z.; Poupko, R.; Samulski, E. T. *J. Chem. Phys.* **1981**, *74*, 5825.
(16) Shiotani, M.; Freed, J. H. *J. Phys. Chem.* **1981**, *85*, 3873. Schwartz, L. J.; Meirovitch, E.; Ripmeester, J. A.; Freed, J. H. *J. Phys. Chem.* **1983**, *87*, 4453.
(17) Spiess, H. W.; Sillescu, H. *J. Magn. Reson.* **1981**, *42*, 381.
(18) Vega, A. J.; Luz, Z. *J. Chem. Phys.* **1987**, *86*, 1803. Poupko, R.; Luz, Z.; Vega, A. J.; Zimmermann, H. *J. Chem. Phys.* **1987**, *86*, 5358.

Table III. Values of Angles (in Deg) Related to the Molecular Structure of TBCN and Its Side Chains (see Figure 6)

angles	solid[a] (cryst.)	P_A I-8 (NMR)	nem. soln I-8 (NMR)	P_C II-13 (NMR)	nem. soln II-13 (NMR)
β^{in}	33.0	35.0	38.2[b]	33.6	36.7[b]
			37.9[c]		36.3[c]
β^{ou}	71.0	71.5	65.3[b]	73.2	69.0[b]
			66.8[c]		69.7[c]
$\angle D^{in}CD^{ou}$	103.3	106.5	103.5[b]	106.8	105.7[b]
			104.7[c]		106.0[c]
β^+		34.7	25.0–26.6[d]		
			36.8–40.7/80.8–72.3[e,f]		
β^-		48.2	37.6–37.8/78.0–78.7[d,f]		
			46.3–47.1/64.3–63.1[e,f]		

[a] Average values taken from crystallographic data in ref 10–12. [b] Mean value in phase V. [c] Mean value in ZLI2452. [d] In phase V over the temperature range 40–50 °C. [e] In ZLI2452 over the temperature range 34–100 °C. [f] The double values correspond to the two possible solutions for β corresponding to positive and negative signs for the relative splittings of $(\langle\nu_Q^l\rangle)/(\langle\nu_Q^{ar}\rangle)$.

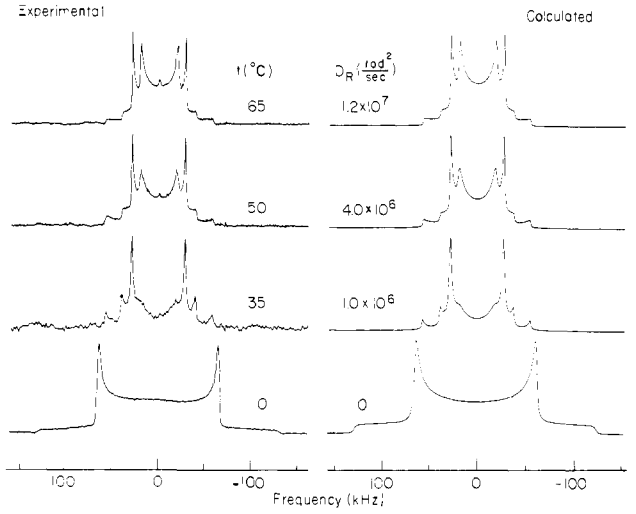

Figure 5. As in Figure 2, but for the crown-ring deuterons of (I-8)[ii] in the solid (bottom traces) and the P_A mesophase. The simulated traces were calculated by superposing dynamic powder patterns due to two deuterons with different β's but identical dynamic parameters as indicated in the figure. The magnetic and geometrical parameters used in the calculations are given in Tables II and III.

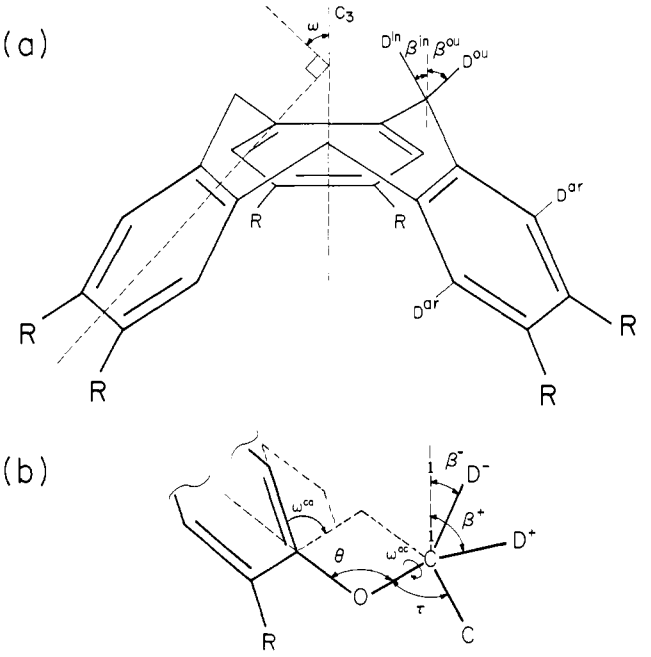

Figure 6. Definitions of some bond and dihedral angles related to (a) the rigid part of the TBCN core, and (b) the first few atoms of an alkyloxy side chain. ω^{co} is the dihedral angle between the aromatic plane and the OC bond and ω^{oc} the dihedral angle between the C^{ar}–O and C^{α}–C^{β} bonds. β^+ and β^- are the angles between the C_3 axis and the corresponding C–D bonds.

state spectrum of these methylene deuterons is also characteristic of the static case with quadrupole interaction parameters, ν_Q = 132 kHz and $\eta \approx 0$. Transition to P_A is accompanied by a discontinuous change, yielding a complicated spectrum, which continues to change as the temperature is further increased within the mesophase. To simulate these spectra, on the basis of the same dynamic model used for the aromatic deuterons, we note that each crown-ring methylene contains two inequivalent deuterons, D^{in} and D^{ou}, whose C–D bonds make different tilt angles, β, to the molecular C_3 axis as indicated in Figure 6a. Consequently, the molecular reorientation which sets in upon transition to the P_A mesophase affects differently the spectrum of the two deuterons, resulting in a superposition of two dynamic powder patterns corresponding to identical magnetic and kinetic, but different geometric, parameters.

We have used the same procedure to fit the experimental spectra of the crown-ring deuterons as used for the aromatic nuclei taking the β's of the inner and outer deuterons as additional adjustable parameters (see Appendix). Examples of such best-fit spectra are shown in the right column of Figure 5. They were calculated using the magnetic parameters given in Table II and diffusion constants, D_R, as plotted in Figure 3. As may be seen the results fall on the same Arrhenius plot as those obtained from the aromatic deuterons. The best-fit β's, β^{in} = 35.0° and β^{ou} = 71.5° (see Table III), are in good agreement with those estimated on the basis of crystallographic data (β^{in} = 33.0°; β^{ou} = 71.0°), as well as with NMR results in nematic solvents as discussed below.

3. NMR Spectra of (I-8)[i] and (I-8)[ii] in Nematic Solvents. To obtain independent estimates for the angles β^{in} and β^{ou} we determined the average quadrupole splittings of the crown-ring and aromatic deuterons in mixtures of (I-8)[i] and (I-8)[ii] dissolved in nematic solvents.[19] Examples of spectra are shown in traces a and b of Figure 7. Each spectrum consists of a doublet due to the aromatic (ar) deuterons and two additional pairs of lines due to the inner and outer (in and ou) crown-ring deuterons, as indicated in the figure. Assuming axially symmetric quadrupole tensors for both types of deuterons, the observed overall doublet splitting in the nematic solutions, $\langle\langle\nu_Q^l\rangle\rangle$, for the various deuterons, l, is given by

$$\langle\langle\nu_Q^l\rangle\rangle = S\nu_Q^l\tfrac{1}{2}(3\cos^2\beta^l - 1) \qquad l = \text{in, ou, or ar} \quad (1)$$

where the double brackets indicate the additional orientational averaging in the nematic solvent. For the aromatic deuterons $\beta^{ar} = \pi/2$, so that the crown-ring β's can be calculated from the relation

$$\left|\frac{\langle\langle\nu_Q^l\rangle\rangle}{\langle\langle\nu_Q^{ar}\rangle\rangle}\right| = \frac{\nu_Q^l}{\nu_Q^{ar}}|(3\cos^2\beta^l - 1)| \qquad l = \text{in or ou} \quad (2)$$

(19) Emsley, J. W.; Lindon, J. C. *NMR Spectroscopy Using Liquid Crystals Solvents*; Pergamon Press: Oxford, 1975. Doane, J. W. In *Magnetic Resonance of Phase Transitions*; Owens, F. J., Pool, C. P., Jr., Farach, H. A., Eds.; Academic Press: New York, 1979.

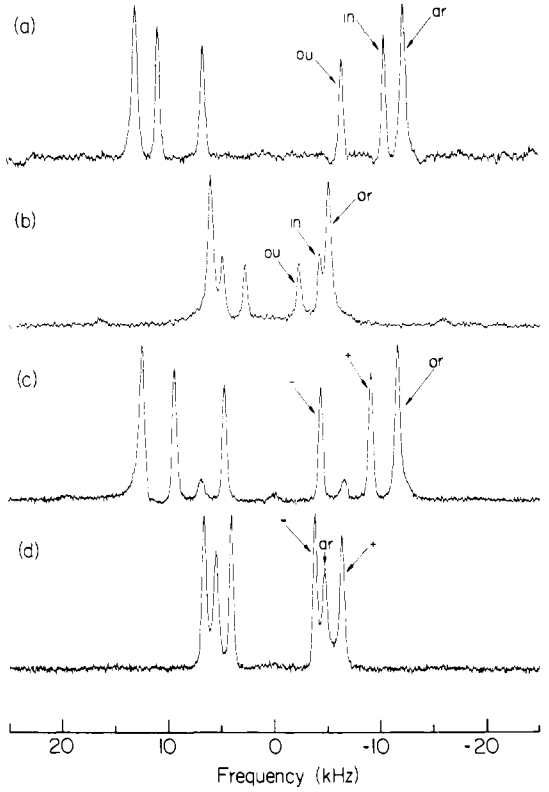

Figure 7. Deuterium NMR spectra of deuterated I-8 isotopomers dissolved in nematic solvents at 40 °C: (a) a mixture of $(I\text{-}8)^{i}$ (0.41 wt %) and $(I\text{-}8)^{ii}$ (0.47 wt %) in ZLI2452, (b) a mixture of $(I\text{-}8)^{i}$ (0.50 wt %) and $(I\text{-}8)^{ii}$ (0.35 wt %) in phase V, (c) a mixture of $(I\text{-}8)^{i}$ (0.80 wt %) and $(I\text{-}8)^{iii}$ (0.35 wt %) in ZLI 2452, (d) a mixture of $(I\text{-}8)^{i}$ (0.60 wt %) and $(I\text{-}8)^{iii}$ (0.60 wt %) in phase V.

provided the splittings are measured in the same solution. Note that absolute values are used since the signs of the average quadrupole interactions cannot be determined from the observed spectra. The results obtained for the β's (using ν_Q^l = 130 kHz, ν_Q^{ar} = 135 kHz) in two different nematic solvents are summarized in Table III. In the calculations of the β's, out of the four possible pairs of results from each spectrum, we selected that pair for which the sum $\beta^{in} + \beta^{ou} = \angle D^{in}CD^{ou}$ is closest to the tetrahedral angle, as expected for a methylene group.

It may be noted in Table III that there are minor variation in the values of β^{in}, β^{out}, and consequently also in the $D^{in}CD^{ou}$ angle in the various systems studied. We have also measured these angles in the first homologue of series I, i.e., hexamethoxytribenzocyclononene, in the two nematic solvents used for the other compounds yielding for β^{in}, β^{ou} (and $\angle D^{in}CD^{ou}$), 37.4°, 67.1° (104.5°) in phase V, and 37.4°, 67.5° (104.9°) in ZLI2452. The small variations in the calculated angles may reflect small structural changes in the TBCN core, but they may also be due to the effect of the side chains on the molecular ordering. If the side-chain isomerization is included in the considerations of ordering in the mesophases, it must be noted that most isomers do not have threefold symmetry, and therefore the simple relations expressed in eq 1 and 2 do not strictly apply. We believe that this effect is insignificant, but it may account for the small variation in the values of the angles calculated from the experimental results.

4. Side-Chain α-Methylene Deuterons. Finally we discuss the deuterium NMR spectra of I-8 labeled in the α-methylene position, $(I\text{-}8)^{ii}$. Experimental results are shown in Figure 8. The solid-state spectrum is again typical of a rigid C–D bond with ν_Q = 117 kHz. This is very close to the usual static quadrupole interaction parameter for aliphatic deuterons and indicates that in the solid not only the central core is static, but also the α carbon and perhaps the rest of the side-chain carbons as well. On transforming to P_A there is a discontinuous change in the spectrum to give a line shape that can again be understood in terms of a

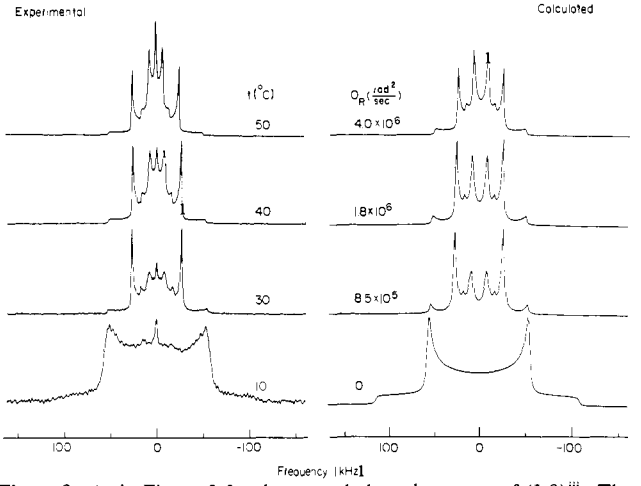

Figure 8. As in Figure 2 for the α-methylene deuterons of $(I\text{-}8)^{iii}$. The simulated spectra (on the right) were computed as a superposition of two powder patterns with the D_R's given in the figure, and magnetic and geometrical parameters summarized in Tables II and III. The weak central peak is due to an isotropic signal of unknown origin.

superposition of two dynamic powder patterns, which continue to evolve upon increasing the temperature within the P_A mesophase. (There is also a weak isotropic peak of unclear origin.) In the high-temperature region the spectrum appears as a superposition of two axially symmetric powder patterns with average quadrupole interaction parameters (at 50 °C) of $|\langle\langle \nu_Q^1 \rangle\rangle|$ = 49.3 kHz and $|\langle\langle \nu_Q^2 \rangle\rangle|$ = 16.0 kHz. These values decrease slightly upon further heating. They reflect averaging over various motions including the fast fluctuations of the molecular C_3 axis, reorientation of the molecules about C_3, and in principle also chain isomerization. However, the fact that the two subspectra of the α-methylene deuterons give, at high temperatures, uniaxial patterns suggests very strongly that no chain isomerization (at least up to the second carbon) takes place even in the P_A mesophase. Such a process will generally give an average biaxial quadrupole tensor, and only in very special cases, e.g., symmetric three- (or four-) site jumps, which are very unlikely in the present situation, will an average uniaxial tensor be obtained.[20] Assuming then that the averaging of the quadrupole interaction of the α-deuterons reflects only the fast fluctuations of the C_3 axis and the molecular reorientational diffusion, we can again fit the experimental spectra using the same model employed above for the aromatic and crown-ring deuterons. Results of such simulations are shown in the right column of Figure 8. In the simulation the diffusion rates were taken from Figure 3, and only two tilt angles, β^+ and β^-, and a common molecular order parameter, S, were taken as adjustable parameters. The latter parameter was found to be somewhat less than that obtained for the rigid core deuterons (see Table II), and also slightly temperature dependent, suggesting that the side chains undergo additional fluctuations, beyond those in which the pyramidic core is involved.

The two tilt angles β^+ and β^- derived from the analysis (Table III) give the C–D bond directions of the two α-methylene deuterons relative to the molecular symmetry axis, C_3 (see Figure 6). The fact that they exhibit just two distinct spectra indicates that all side chains are similarly oriented with respect to the rigid core. In fact, the values of β^+ and β^- are related to the conformation of the side chains and can therefore provide additional structural information. Straightforward, although somewhat cumbersome, calculations[21] give the following relations between

(20) Lifshitz, E.; Goldfarb, D.; Vega, S.; Luz, Z.; Zimmermann, H. *J. Am. Chem. Soc.* **1987**, *109*, 7280.

(21) Poupko, R.; Luz, Z.; Zimmermann, H. *J. Am. Chem. Soc.* **1982**, *104*, 5307.

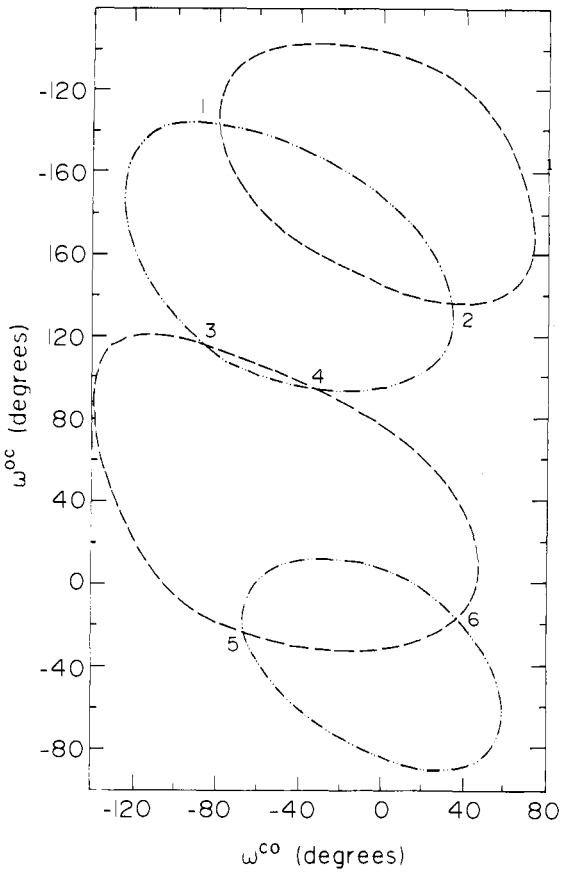

Figure 9. Graphical solution of ω^{co} and ω^{oc} for I-8 in the P_C mesophase. The two sets of contours are the solutions of eq 3 for the experimental values of $\beta^+ = 34.7°$ (dashes and dots), and $\beta^- = 48.2°$ (dashes). Their intersections give the desired possible solutions for the dihedral angles and are summarized in Table IV. For the calculation the following angles were used (see Figure 6): $\omega = 43.0°$, $\theta = 117.0°$, $\tau = 109.5°$.

Table IV. The Possible Pairs of Dihedral Angles ω^{co} and ω^{oc} Obtained by Solving Eq 3 for the Experimental Values of β^+ and β^- (Table III)[a]

	1	2	3	4	5	6
ω^{co}	−81.7	33.4	−89.4	−32.4	−67.5	41.0
ω^{oc}	−136.2	137.7	116.5	96.2	−25.0	−14.6

[a] The labeling of the various solutions are as indicated in Figure 9.

β^+ and β^-, and the dihedral angles ω^{co} and ω^{oc} of the C^{ar}–O and O–C^{α} bonds of the side chains

$$\cos\beta^{\pm} = -\tfrac{1}{2}\sin\omega\,[\sin\theta\cos\omega^{co}\cos\tau + \sin\omega^{co}\sin\tau\sin(\omega^{oc} \pm 2\pi/3) + \cos\theta\cos\omega^{co}\sin\tau\cos(\omega^{oc} \pm 2\pi/3) + \sqrt{3}\cos\theta\cos\tau - \sqrt{3}\sin\theta\sin\tau\sin(\omega^{oc} \pm 2\pi/3)] - \cos\omega\,[\sin\theta\sin\omega^{co}\cos\tau - \cos\omega^{co}\sin\tau\sin(\omega^{oc} \pm 2\pi/3) + \cos\theta\sin\omega^{co}\sin\tau\cos(\omega^{oc} \pm 2\pi/3)] \quad (3)$$

where the definitions of the various angles are given in Figure 6. To solve this equation for ω^{co} and ω^{oc}, we have used the following graphical procedure. Contours of ω^{co} versus ω^{oc}, which solve eq 3 for the particular β^+ determined from the NMR spectra, using $\omega = 43.0°$, $\theta = 117.0°$, $\tau = 109.5°$, are plotted as dashes and dots in Figure 9. These contours correspond to all possible pairs of dihedral angles ω^{co} and ω^{oc} which result in a tilt angle β^+ for the deuteron D^+. Similarly the dashed curves in Figure 9 correspond to all possible pairs of ω^{co} and ω^{oc} which yield a tilt angle identical with the experimentally determined value β^- for the second deuteron, D^-. Consequently, the intersections of the two sets of curves give the desired solutions for the possible pairs of dihedral angles which simultaneously result in a tilt angle β^+ for one deuteron (D^+), and β^- for the second deuteron (D^-). As may be seen there are six different pairs of solutions consistent with the experimental results. They are summarized in Table IV according to the labeling in Figure 9. Without further experiments no decision between these solutions is possible. However, by considering molecular models some solutions can be deemed as less likely conformations due to steric hindrance. In particular those conformations in which the chains are folded toward the inner side of the TBCN core (solutions 5 and 6) can be rejected. Such considerations suggest as the more likely conformations solutions 1, 3, where the chains start in a perpendicular outward orientation, or solutions 2, 4, where they start at a coplanar direction.

Table V. Experimental and Calculated *d*-Spacings for the P_C Mesophase of II-13 Indexed on a Two-Dimensional Hexagonal Lattice with $a = 52.77$ Å

Miller indices *hk*	*d*(meas)[a] (Å)	*d*(calc) (Å)
11	26.46 (0.04)	26.38
20	22.81 (0.03)	22.85
21	17.38 (0.14)	17.27
22	13.21 (0.10)	13.19
32	10.41 (0.06)	10.48
42	8.60 (0.02)	8.64
(−)[b]	4.5	

[a] Average values over the mesophase region. (Numbers in parentheses are rms deviations from the average values.) [b] This line corresponds to the intracolumnar stacking distance of the molecules.

To complete this section, we briefly discuss the deuterium NMR spectra of $(I\text{-}8)^{iii}$ in nematic solvents. In traces c and d of Figure 7 are depicted spectra of mixtures of $(I\text{-}8)^{i}$ and $(I\text{-}8)^{iii}$ in ZLI2452 and in phase V, respectively. In both solutions $(I\text{-}8)^{iii}$ exhibits two intense pairs of lines due to the two inequivalent α-methylene deuterons. In trace c there is an additional weak pair of peaks which may be due to a low-abundance conformational isomer which is in slow exchange with the dominant species. As may be seen, the splittings of the α-methylene signals relative to those of the aromatic deuterons are completely different in the two solvents and, in fact, also strongly temperature dependent. This indicates that contrary to the situation in the neat phases of I-8, in nematic solutions, fast chain isomerization does occur and consequently affects the dihedral angles ω^{co} and ω^{oc}. The calculated values of β^+ and β^- (using eq 2 with $\nu_Q^l = 117$ kHz) for these solutions, Table III, are therefore not very meaningful and represent weighted averages over the distribution of the side-chain conformers. Note that ranges of results are given for β^+ and β^- corresponding to the range of temperature over which the measurements were made in both nematic solvents. Also note that when $|\langle\langle\nu_Q^l\rangle\rangle| < |\langle\langle\nu_Q^{ar}\rangle\rangle|$ there are two possible solutions for β corresponding to positive and negative relative signs.

II. Hexaalkanoyloxytribenzocyclononene (Series II-*n*). A. X-ray Measurements. Of the II-*n* series only the homologue II-13 was investigated in the present work using both the X-ray and NMR techniques. Its phase diagram is:

$$K_1 \xrightarrow{67.4\ °C} P_D \xrightarrow{99.9\ °C} P_C \xrightarrow{139.2\ °C} L$$

where P_D and P_C are respectively biaxial and uniaxial mesophases. These mesophases were previously studied by Levelut et al. using X-ray diffraction in the two homologues II-10, which exhibits only P_D, and II-12, which like II-13 exhibits both P_D and P_C. They interpreted their results for P_D and P_C in terms of a 2D oblique phase with two molecules per unit cell and a 2D hexagonal phase with four molecules per unit cell, respectively. We have extended these measurements to the P_D and P_C mesophases of II-13, and in Figure 1 we reproduce typical diffraction patterns. In both phases, in addition to the low-angle diffraction peaks shown in the figure, a broad peak is also observed corresponding to 4.4 to 4.5 Å which, as for P_A, is ascribed to the stacking distance of the molecules within the columns. In the high-temperature P_C mesophase, this line broadens even more with temperature, indicating an increase in disorder of the stacking as the clearing point is approached. Otherwise within each mesophase the diffraction pattern is essentially independent of temperature.

of the potential seen in Figures 2–4 could be induced by rapid destruction of the monolayer structure. Previously, we[9] proposed a mechanism of successive formation and abrupt destruction of the monolayer structure. The oscillation described in this report may be explained in a similar manner, as shown schematically in Figure 9. After the induction period (State I), a first pulse is generated (State II) and repeated interchange of States III and IV occurs.

State I: CTA cations, which are mainly present as micelles in the aqueous phase, move toward the interface and become situated at the interface. Simultaneously molecules of picric acid move toward the interface and dissolve in the aqueous phase. Thus the concentrations of CTA cations and picrate anions around the interface increase gradually, and CTA cations tend to form a monolayer at the interface.

State II: When the concentration of CTA cations at the interface reaches a critical value, CTA cations are abruptly transferred to the organic phase with formation of inverted micelles.

State III: When the concentration of CTA^+ on the interface decreases to a lower critical value, accumulation of CTA^+ on the interface begins again with gradual formation of a monolayer.

State IV: When the concentration of CTA^+ increases to an upper critical value, abrupt transfer of CTA cations to the organic phase occurs.

Effects of Alcohols on the Oscillation. In the Experimental Section it was shown that the dependence of the frequency of oscillations on the concentration of an alcohol apparently follows the relationship of Langmuir's adsorption isotherm (eq 1). It was also found that the critical concentration needed to induce the oscillation depends on the hydrophobicity of the alcohol (eq 2). These effects of alcohols on the oscillation require consideration. It is well known that alcohols decrease the cmc of amphiphilic molecules.[20] This decrease is due to incorporation of the alcohol into the micelle, which changes the manner of aggregation of the amphilic molecules. Alcohols certainly affect the structure of the CTA^+ monolayer on the interface.[21] They may also influence the rate of migration of CTA cations from the aqueous phase to the interface and from the interface to the organic phase. These effects of alcohols may induce change in the frequency of oscillations.

The degree of incorporation of alcohols into aggregates of CTA^+ (i.e., the monolayer on the interface, micelles in the aqueous phase, and inverted micelles in the organic phase) probably increases with an increase in the hydrophobicity of the alcohols. If so, this could be related to the fact that the hydrophobicity of alcohols is closely related to the frequency of oscillations.

Comparison with Biological Chemoreceptive Membranes. Application of chemical stimuli to a receptor organ induces nerve impulses. The mechanism of generation of this response is a very interesting problem. In 1954 Beidler[12] proposed a hypothesis to explain taste stimulation based on his finding that the relationship between the magnitude of integrated electrical response of the taste and the concentration of a stimulant satisfies Langmuir's adsorption isotherm; he proposed that adsorption of a chemical stimulant to a taste receptor induces stimulation of the associated sensory neuron. Many lines of evidence support this adsorption hypothesis of taste reception, but the details of the mechanism are still unknown. In the liquid membrane the logarithm of the frequency apparently followed a relationship similar to that of Langmuir's adsorption isotherm, suggesting that the response of the liquid membrane resembles that of the biological chemoreceptive membrane, though details of each mechanism should be different.

Though this study is only a beginning, it indicates the possibilities of developing a new type of chemical sensor capable of distinguishing various chemical substances on the basis of information on the frequency and the shape of impulses.

Conclusions

(1) Sustained oscillations of electrical potential were generated in a liquid membrane consisting of an oil layer, nitrobenzene containing picric acid, imposed between two aqueous phases, one of which contained CTAB and an alcohol.

(2) The frequency of oscillations increased with an increase in the concentration of the alcohol. The logarithm of the frequency apparently obeyed a relationship similar to that of Langmuir's adsorption isotherm.

(3) The threshold concentration needed to induce the oscillation decreased with an increase in the hydrophobicity of the alcohol. The relationship between the critical concentration and the hydrophobicity can be represented by the following equation

$$\log C_{th} = -a \log P + b$$

where C_{th} is the concentration where the oscillations change sharply, P is the partition coefficient of the alcohol between benzene and water, and a and b are constants.

(4) The oscillatory phenomenon can be explained by a mechanism of repetitive formation and destruction of a monolayer of CTA^+ at the interface.

(5) The manner of the electrical response of the liquid membrane resembles that of biological chemoreceptive membranes.

(6) The possibility of developing a new type of chemical sensor that can distinguish various chemical substances on the basis of information on the frequency and shape of impulses is suggested.

Acknowledgment. We thank Professor T. Ota for encouragement. It is a pleasure to acknowledge the stimulating discussion and helpful suggestions of Dr. H. Terada and Professor H. Uedaira. This work was supported by a Grant-in-Aid for Scientific Research to K.Y. from the Ministry of Education, Science and Culture of Japan.

Registry No. CTAB, 57-09-0; methanol, 67-56-1; ethanol, 64-17-5; isopropyl alcohol, 67-63-0; *n*-propyl alcohol, 71-23-8; *n*-butyl alcohol, 71-36-3; *n*-pentyl alcohol, 71-41-0; benzyl alcohol, 100-51-6; nitrobenzene, 98-95-3; picric acid, 88-89-1.

(20) Tanford, C. "The Hydrophobic Effect: Formation of Micelles and Biological Membranes"; John Wiley & Sons: New York, 1980; pp 90–95.
(21) Ahmad, S. I.; Friberg, S. *J. Am. Chem. Soc.* **1972**, *94*, 5196–5199.

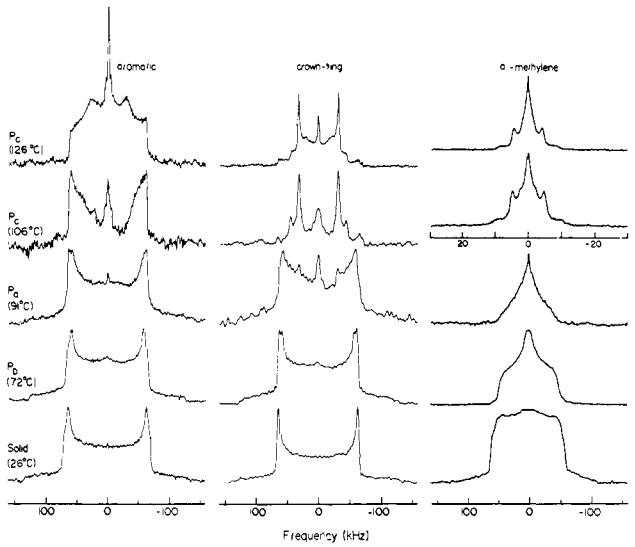

Figure 10. Deuterium NMR spectra of three deuterated species of II-13 in the solid, P_D and P_C phases. All spectra were recorded on heating from the solid at the indicated temperatures and phases using the quadrupole echo method. The spectra in the columns, from left to right, correspond to aromatic deuterons in $(II\text{-}13)^{i}$, crown-ring methylene deuterons in $(II\text{-}13)^{ii}$, and the side-chain α-methylene deuterons in $(II\text{-}13)^{iii}$. Note the expanded scale used to record the spectra of $(II\text{-}13)^{iii}$ in the P_C mesophase.

only 11 reflections, and the addition of an extra adjustable parameter naturally improves the fit. We also note that a comparable fit could be obtained for the three-dimensional $P2_12_12_1$ structure. Since, however, the X-ray diffraction intensity pattern and the optical microscopy observation on P_D suggest a liquid-crystalline structure, we continue the discussion on the basis that it consists of a two-dimensional array of columns.

To do so we first compare our results for II-13 with those obtained by Levelut et al.[4] for II-10 (which exhibits only P_D) and II-12 (which like II-13 exhibits both P_D and P_C). The lattice parameter reported for P_C of II-12 is a = 49.38 Å which compares well with 52.77 Å for II-13. The parameters reported for P_D in II-10 and II-12 are:

$$\text{II-10: } a = 34.35 \text{ Å}, b = 25.49 \text{ Å}, \gamma = 99.1°$$

$$\text{II-12: } a = 38.57 \text{ Å}, b = 27.26 \text{ Å}, \gamma = 95.5°$$

and must be compared to our values of a = 68.6 Å, b = 53.2–53.6 Å for the two-dimensional lattices of II-13 (see Table VI). These values are almost exactly twice as large as those calculated for II-10 and II-12 by Levelut et al. We have therefore reexamined their data for the P_D mesophase, for a possible fit to a 2D-oblique lattice of double the size used by them, yielding

$$\text{II-10: } a = 69.68 \text{ Å}, b = 52.03 \text{ Å}, \gamma = 99.1°, \text{ rms} = 0.06 \text{ Å}$$

$$\text{II-12: } a = 76.97 \text{ Å}, b = 54.70 \text{ Å}, \gamma = 95.5°, \text{ rms} = 0.14 \text{ Å}$$

The rms deviations of these analyses are comparable to those calculated for the structures proposed by Levelut et al., leaving the question open as to whether there are eight or two columns per unit cell, or whether perhaps in the lower homologues there are eight while in II-13 (and in the higher homologues) there are six.

B. NMR Measurements. As indicated above we have also performed deuterium NMR measurements on a number of specifically deuterated II-13 isotopomers. These include compounds labeled in the unsubstituted sites of the aromatic rings $(II\text{-}13)^{i}$, in the crown-ring methylene, $(II\text{-}13)^{ii}$, and in the α-methylene of the side chains $(II\text{-}13)^{iii}$. Examples of spectra recorded in the solid and in the two mesophases are shown in Figure 10. We have analyzed the results in much the same way as for the I-8 isotopomers, although not as comprehensively. We therefore provide a less extensive analysis of these results and for convenience divide the discussion according to the three phases of II-13, i.e., solid, P_D, and P_C.

1. The Solid Phase. The NMR spectra of the rigid core (aromatic and crown-ring) deuterons in the solid phase are again typical of a static system with quadrupole interaction parameters (see Table II) similar to those observed in solid I-8. The spectrum of the α-methylene deuterons in this phase is also solid-like, but the typical features of rigid powder spectra are less pronounced and suggest that some slow motion involving the α-carbons already occurs in the solid state. Since this process does not involve the rigid core it must correspond to slow fluctuations or isomerization of the side chains.

2. The P_D Mesophases. The line shapes of the aromatic and crown-ring deuterons in this phase are still solid-like indicating that no fast reorientational diffusion of the mesogen molecules takes place in P_D. There is, however, a small reduction in the overall quadrupole splitting of both deuterons, corresponding to S = 0.93 (see Table II). This is again most likely because of fast fluctuations of the long axes of the columns forming the mesophase as was assumed for I-8. Note, however, that despite this partial averaging the aromatic deuteron spectra still exhibit a small asymmetry parameter, reflecting the biaxial nature of the P_D mesophase. The perpendicular features of the crown-ring deuterons exhibit a small splitting which we are unable to explain and could very well be due to the presence of impurities in this particular sample. The appearance of this sample was quite dark, but we were unable to purify it by repeated crystallization.

The α-methylene spectra in the P_D mesophase differ from those in the solid, and exhibit a powder pattern with a large asymmetry parameter ($\eta \approx 1$) and a highly reduced quadrupole interaction $\langle\langle \nu_Q \rangle\rangle \approx 50$ kHz (see Table II). This line shape clearly indicates the presence of fast although still highly restricted chain isomerization in this phase. The data are, however, not sufficient to identify the exact mechanism of this process. It could very well be similar to the two-site jump model proposed to interpret the line shapes observed in the solid phases of benzenehexaalkanoate.[20]

3. The P_C Mesophase. Transition from P_D to P_C results in a discontinuous change in the spectra of all three types of deuterons (see Figure 10). The spectra of the aromatic and crown-ring deuterons in this phase are very similar to those observed in the P_A mesophase of I-8 and can, in fact, be interpreted in much the same way, i.e., in terms of planar reorientation about the molecular C_3 axis. We have accordingly analyzed the spectra of the aromatic deuterons of II-13, and the best-fit results for D_R are plotted in Figure 3. The derived kinetic parameters, using the entries given in Table II, are $D_R(373 \text{ K}) = 1.4 \times 10^5 \text{ rad}^2/\text{s}$ and ΔE = 112 kJ/mol. The activation energy for reorientation is thus somewhat higher than for I-8, and the rate at room temperature considerably slower, reflecting the much longer chain in II-13 compared to that in I-8. The spectra of the crown-ring deuterons are in qualitative agreement with the results of the aromatic deuterons. They correspond to a superposition of two dynamic powder patterns due to the inner and outer deuterons as in I-8. The values of β^{in} and β^{ou} quoted in Table III for these deuterons were estimated from the $(II\text{-}13)^{ii}$ spectra at high temperatures, but no quantitative dynamic analysis was performed. Note that the dynamic range of the diffusion is such that over a considerable range of temperatures the spectrum of the outer deuterons is washed out because of significant line broadening, while the signal of the inner deuterons remains sharp. This deceptively simple appearance of the spectra hampered their interpretation at the early stages of the work.

The transition to P_C is also accompanied by a significant change in the line shape and overall width of the spectra due to side-chain α-methylene deuterons. They exhibit a line shape corresponding to a superposition of two powder patterns, one with an axially symmetric average quadrupole tensor, while the other appears to have an asymmetric parameter close to 1 (see Table II). The change in the overall spectral width for both deuterons is much larger than would be expected from the reorientational diffusion alone, indicating that the α-deuterons are involved in additional dynamic processes in this phase. They undoubtedly reflect fast

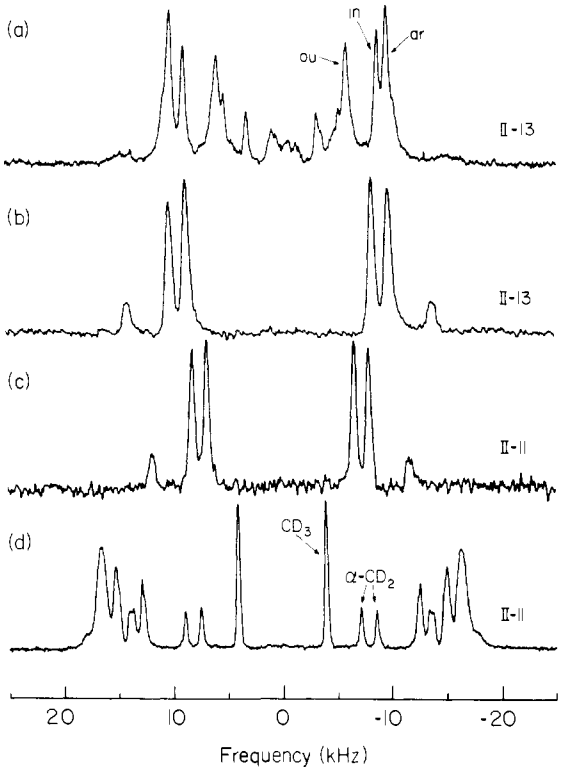

Figure 11. Deuterium NMR spectra of deuterated II-13 and II-11 species dissolved in nematic phase V: (a) a mixture of $(II\text{-}13)^{i}$ (0.3 wt %) and $(II\text{-}13)^{ii}$ (0.3 wt %) at 50 °C, (b) $(II\text{-}13)^{iii}$ (0.5 wt %) at 42 °C, (c) II-11 deuterated in the side-chain α-methylene (0.5 wt %) at 52 °C, (d) II-11 perdeuterated in the side chain (0.5 wt %) at 47 °C.

conformational isomerization of the side chains; however, their complete identification cannot be done on the basis of these spectra alone.

4. Deuterium Spectra in Nematic Solvents. As for the I-8 compound we have also recorded the deuterium spectra of II-*n* deuterated species in nematic solvents. In trace a of Figure 11 is shown a spectrum of a mixture of $(II\text{-}13)^{i}$ and $(II\text{-}13)^{ii}$ dissolved in nematic phase V from which the angles β of the crown-ring deuterons can be calculated. The results (Table III) were already discussed in connection with the corresponding values derived from solutions of I-*n* homologues.

Traces b and c are of the side-chain α-methylene deuterons in II-13 and II-11, respectively. Both show two intense doublets and a weak pair of lines as was also observed for I-8. Also shown in Figure 11 (trace d) is a spectrum of a solution of chain perdeuterated II-11 in a nematic solvent. The signals due to the end methyl groups and the two α-methylenes (as indicated) can readily be identified from their relative intensities and by comparison with spectra of specifically deuterated species. The rest of the peaks must be due to the other eight methylene groups. We have not yet analyzed these results for the possible chain conformations, but it is worth indicating two characteristic features in which the present spectrum differs from those commonly observed for aliphatic side chains in liquid crystalline mesophases. The most conspicuous difference is in the relative splitting of the α-methylene deuterons which usually are the largest of all methylenes,[22,23] while here they are the smallest. The other point concerns the relative splitting of the methyl deuterons. These are generally far smaller than the rest of the chain deuterons owing to (i) the decrease in orientational order along the chain and (ii) the fast reorientation of the methyl group about its C_3 axis. The latter effect reduces the deuterium splitting by a factor of 3. If we multiply the observed methyl splitting of II-11 by 3, we obtain an effective splitting of the same order as for the rest of the methylenes. These anomalies are certainly related to the special shape of the rigid core, but as indicated we have not yet quantitatively analyzed these results.

(22) Hsi, S.; Zimmermann, H.; Luz, Z. *J. Chem. Phys.* **1978**, *69*, 4126.
(23) Goldfarb, D.; Luz, Z.; Zimmermann, H. *J. Chem. Phys.* **1983**, *78*, 7065.

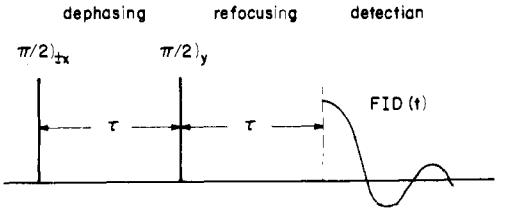

Figure 12. The quadrupole echo pulse sequence and definitions of the time intervals.

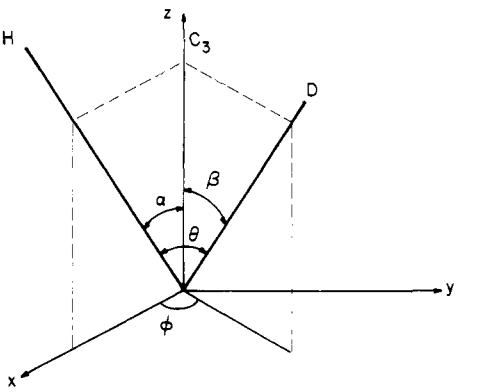

Figure 13. The coordinate system and definitions of the C–D bond angles (identified with the principal direction of the quadrupole interaction tensor) used in the text. H is the direction of the magnetic field, D the direction of the C–D bond, θ the angle between these two directions, and α the polar angle of H (assumed to be in the xz plane); β and ϕ are the polar and azimuthal angles of the C–D bond.

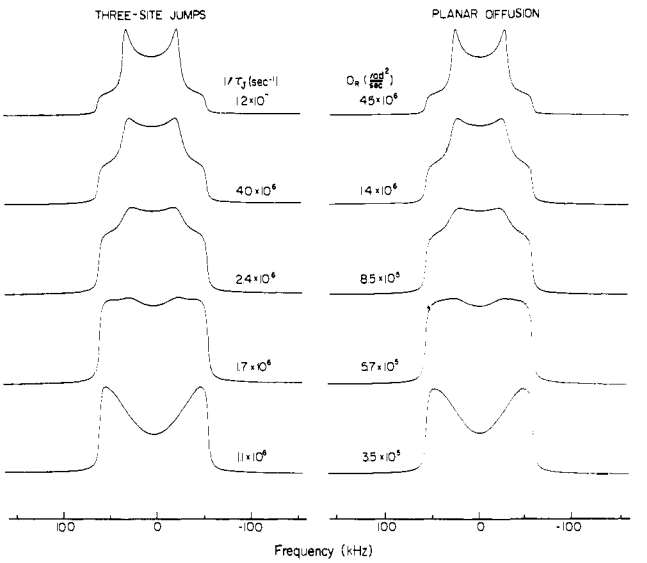

Figure 14. Comparison of simulated powder spectra calculated for the three-site jump model (left) and rotational diffusion (right) for the indicated dynamic parameters. The other parameters were $\langle\nu_Q\rangle$ = 115 kHz, $1/T_2 = 10^4$ s^{-1}, τ = 20 μs. The pairing of the spectra was chosen so as to emphasize the similarity in the evolution of the spectra in both models.

Summary and Conclusions

Although the pyramidic mesophases of the TBCN derivatives may on the basis of X-ray and optical microscopy be classified as liquid crystalline, their high order and very low mobility render them very similar to "soft solids". Most discotic liquid crystals of molecular weights similar to those of the pyramidic compounds studied here exhibit mesophases with considerably higher mobility. Otherwise, however, the pyramidic mesophases are quite similar

to the usual discotics. They exhibit undulations of the columnar axes, molecular reorientation, and probably also molecular translation between columns, although the latter was not reflected in the NMR results. The stiffness of these mesophases is also reflected in the relatively high rigidity of the side chains. It appears that alkyloxy side chains do not undergo conformational isomerization on the NMR timescale, at least as far as the first three atoms in the chain are concerned. The alkanoyloxy side chains are more mobile, although in P_D they appear to be quite restricted.

The interesting question concerning the relative polarity of neighboring columns, or of the stacking of the molecules within the columns, could not be studied by the NMR method. The problem of whether the mesophases are ferroelectric or antiferroelectric thus remains open. It can in principle be determined by dielectric measurements on single domains or dielectric relaxation dispersion. The high viscosity of these phases and the difficulty of aligning them render, however, such experiments quite difficult.

Acknowledgment. This research was supported by a grant from the German-Israeli Foundation (GIF) for Scientific Research and Development, by the National Council for Research and Development, Israel, by the KFA Jülich, and by the Israel Academy of Sciences.

Appendix

In this Appendix we describe the computation procedure used to simulate the dynamic NMR line shapes due to planar reorientation discussed in the main text. It is a generalization of a previously introduced method to calculate dynamic line shapes due to molecules undergoing planar reorientation in connection with deuterium spectra in cholesteric materials.[15] It differs from the earlier treatment in two respects. First, the model is extended to cases in which the C–D bond is not necessarily perpendicular to the reorientation axis, but rather inclined at a general angle to this axis. This extension is necessary for the simulation of the spectra of the crown-ring and α-methylene deuterons discussed in the main text. The analogous case for the anisotropic chemical shift tensor was treated by Vega and English[24] in their study of poly(tetrafluoroethylene) by ^{19}F NMR. The second point refers to an experimental aspect; rather than using single pulses (as was the case in the earlier work), here the NMR signals are recorded by the quadrupole echo method (see Figure 12). An exact simulation of dynamic spectra obtained in such experiments requires the computation of the time evolution of the density matrix during all stages of the quadrupole echo experiment, starting immediately after the first pulse, through the dephasing and refocusing periods and finally during the detection.

We discuss rigid molecules with 3-fold symmetry, such as TBCN, aligned in a uniaxial liquid crystalline domain with the molecular symmetry axis parallel to the director and undergoing a reorientational motion about their C_3 axis. The coordinate system and relevant angles are defined in Figure 13. Two different reorientation mechanisms are considered: (i) 3-fold jumps in which the molecules reorient by $\pm 2\pi/3$, with a mean lifetime between jumps, τ_J; (ii) planar diffusion characterized by a diffusion constant D_R. The quadrupole interaction tensor of the deuterons is assumed to be uniaxial with a principal component $\langle \nu_Q \rangle$ inclined at an angle β to the C_3 axis. The angular brackets indicate averaging due to fast uncorrelated fluctuations of the C_3 axis about the director. In the TBCN core discussed in the main text, β equals $\pi/2$ for the aromatic deuterons and β^{in} and β^{ou} for the inner and outer crown-ring hydrogens. For the aliphatic chain deuterons, β depends on the conformation of the chain, and if fast chain isomerization takes place, averaging over the conformer distribution must be made.

In the main text we consider spectra obtained from powder samples consisting of an isotropic distribution of domains. Since molecular diffusion between domains is negligible, the simulated spectra of such samples are calculated by integration over the isotropic distribution. Here we consider the spectrum of a single domain with the magnetic field oriented at a general angle α to the director (taken along z), and the principal quadrupole tensor interaction (identified with the C–D bond direction) making the polar angles β and ϕ. With these definitions (see Figure 13) the quadrupole frequency is given by:

$$\langle \nu_Q(\phi) \rangle = \langle \nu_Q \rangle \tfrac{1}{2}[3\cos^2\theta(\alpha,\beta,\phi) - 1] = A + 2B\cos\phi + 2C\cos 2\phi = A + B(e^{i\phi} + e^{-i\phi}) + C(e^{i2\phi} + e^{-i2\phi}) \quad (A1)$$

where $\theta = \theta(\alpha,\beta,\phi)$ is the angle between the magnetic field and the C–D bond, and

$$A = \langle \nu_Q \rangle (\tfrac{3}{2}\cos^2\beta\cos^2\alpha + \tfrac{3}{4}\sin^2\beta\sin^2\alpha - \tfrac{1}{2})$$
$$B = \langle \nu_Q \rangle (\tfrac{3}{8}\sin 2\beta \sin 2\alpha) \quad (A2)$$
$$C = \langle \nu_Q \rangle (\tfrac{3}{8}\sin^2\beta\sin^2\alpha)$$

(i) The 3-Fold Jump Model. In this model we assume jumps of the principal quadrupole axis, or rather of the C–D bond, between three sites having the same polar angle β and varying azimuthal angles ϕ, $\phi + 2\pi/3$, $\phi - 2\pi/3$. Following the procedure outlined in ref 15, this gives for $FID^{\phi}(t)$ the FID signal due to molecules oriented at ϕ, $\phi \pm 2\pi/3$,

$$FID^{\phi}(t) = \mathrm{Re}\tfrac{1}{3}\{\mathbf{1}\cdot\exp[-\mathbf{R}^{\phi}(t+\tau)]\exp(-\mathbf{R}^{\phi}\tau)^{*}\cdot\mathbf{1}\} \quad (A3)$$

where the Liouville matrix $\mathbf{R}^{\phi}$ has the form shown in eq A4. The

$$\mathbf{R}^{\phi} = \begin{bmatrix} i\langle\nu_Q(\phi)\rangle + \frac{1}{\tau_J} + \frac{1}{T_2} & -\frac{1}{2\tau_J} & -\frac{1}{2\tau_J} \\ -\frac{1}{2\tau_J} & i\left\langle\nu_Q\left(\phi+\frac{2\pi}{3}\right)\right\rangle + \frac{1}{\tau_J} + \frac{1}{T_2} & -\frac{1}{2\tau_J} \\ -\frac{1}{2\tau_J} & -\frac{1}{2\tau_1} & i\left\langle\nu_Q\left(\phi-\frac{2\pi}{3}\right)\right\rangle + \frac{1}{\tau_J} + \frac{1}{T_2} \end{bmatrix} \quad (A4)$$

line shape for a particular ϕ can be obtained by analytical Fourier transformation of FID^{ϕ}. Alternatively the FID for the whole domain is first obtained by integrating over ϕ, followed by numerical Fourier transformation.

(ii) The **Planar Diffusion Model.** In the planar diffusion mechanism the molecules are assumed to undergo infinitesimal jumps about their C_3 symmetry axis. Dynamic spectra due to this mode of motion can be computed by several approaches, for example, by dividing the ϕ plane into N segments and allowing jumps between adjacent segments. The spectrum obtained in the limit, $N \to \infty$, corresponds to a diffusion constant D_R, which is related to the jump rate $1/\tau_J$ by $D_R = \pi^2/(8N^2\tau_J)$. This procedure has been applied to single-pulse experiments[15] and can be extended to the quadrupole echo case by straightforward modifications.[18]

A more efficient procedure for calculating the dynamic line shape due to planar diffusion is to make use of the expansion method.[15,16,24-28] We start with the equation of motion of the transverse magnetization generated by the first $(\pi/2)_{-x}$ pulse in the quadrupole echo sequence (Figure 12)

$$\frac{dG(\phi,t)}{dt} = \left[-i\langle\nu_Q(\phi)\rangle + \left(\frac{1}{T_2} - D_R\frac{\partial^2}{\partial\phi^2}\right)\right]G(\phi,t) \quad (A5)$$

where $G(\phi,t)$ corresponds to those deuterons whose principal quadrupole axis has at time t the azimuthal angle ϕ. It consists of a complex combination[18] of the expectation values of the corresponding transverse coherences I_y and J_y

$$G(\phi,t) = y(\phi,t) + ib(\phi,t) \quad (A6)$$

so that the final FID(t) signal is proportional to the real part of the integral over $G(\phi,t)$

$$FID(t) = \mathrm{Re}\int_0^{2\pi} d\phi\, G(\phi,t) \quad (A7)$$

(24) Vega, A. J.; English, A. D. *Macromolecules* **1980**, *13*, 1635.

(25) Freed, J. H.; Bruno, G. V.; Polnaszek, C. F. *J. Phys. Chem.* **1971**, *75*, 3385.

(26) Vega, A. J.; Fiat, D. *J. Magn. Reson.* **1974**, *13*, 260.

(27) Baram, A.; Luz, Z.; Alexander, S. *J. Chem. Phys.* **1976**, *64*, 4321.

(28) Campbell, R. F.; Meirovitch, E.; Freed, J. H. *J. Phys. Chem.* **1979**, *83*, 525.

To solve $G(\phi,t)$, it is expanded in the complete set of exponential functions

$$G(\phi,t) = \sum_{k'=-\infty}^{\infty} a_{k'}(t) \exp(ik'\phi) \tag{A8}$$

so that the FID(t) signal is proportional to $a_0(t)$. Substituting this expression into (A5) and using (A1) gives

$$\sum \frac{da_{k'}(t)}{dt} \exp(ik'\phi) = -iA\sum a_{k'}(t) \exp(ik'\phi) - iB\sum a_{k'}(t) \{\exp[i(k'+1)\phi] + \exp[i(k'-1)\phi]\} - iC\sum a_{k'}(t)\{\exp[i(k'+2)\phi] + \exp[i(k'-2)\phi]\} + \sum(1/T_2 + k^2 D_R)a_{k'}(t) \exp(ik'\phi) \tag{A9}$$

Multiplying by $\exp(-ik\phi)$ and integrating over ϕ results in the following infinite set of coupled equations for the coefficients $a_k(t)$:

$$\frac{da_k(t)}{dt} = -[iA + 1/T_2 + k^2 D_R]a_k(t) - iB[a_{k+1}(t) + a_{k-1}(t)] - iC[a_{k+2}(t) + a_{k-2}(t)] \tag{A10}$$

Adding up the equations for $a_k(t)$ and $a_{-k}(t)$ and defining

$$\begin{aligned} \bar{a}_0(t) &= \sqrt{2}a_0(t) \\ \bar{a}_k(t) &= a_k(t) + a_{-k}(t) \qquad \text{for } k \neq 0 \end{aligned} \tag{A11}$$

allows us to write the equations for the $\bar{a}_k(t)$'s in a compact form, i.e.,

$$d\bar{\mathbf{a}}(t)/dt = -\mathbf{R}\bar{\mathbf{a}}(t) \tag{A12}$$

where $\bar{\mathbf{a}}(t)$ is the column vector of the $\bar{a}_k(t)$'s and $\mathbf{R}$ is an infinite pentadiagonal, symmetric matrix with constant off-diagonal elements (except in the first row and column, eq A13). To solve

$$\mathbf{R} = \begin{bmatrix} iA & i\sqrt{2}B & iC & & & \\ i\sqrt{2}B & \left(iA + \frac{1}{T_2} + D_R + iC\right) & iB & iC & & \\ iC & iB & \left(iA + \frac{1}{T_2} + 4D_R\right) & iB & iC & \\ & & \ddots & \ddots & \ddots & \\ & & & iC & iB & \left(iA + \frac{1}{T_2} + k^2 D_R\right) \end{bmatrix} \tag{A13}$$

for $\bar{\mathbf{a}}(t)$, the matrix $\mathbf{R}$ is truncated at some sufficiently high k value, and the truncated set of the $\bar{a}_k(t)$'s is obtained by integration:

$$\bar{\mathbf{a}}(t') = \exp[-\mathbf{R}(t'-t'')]\bar{\mathbf{a}}(t'') \tag{A14}$$

Following the procedure outlined in ref 18, we can now compute the evolution of the $\bar{a}_k(t)$'s during the quadrupole echo experiment, yielding for the detection period:

$$\bar{\mathbf{a}}(t) = \exp[-\mathbf{R}(\tau + t)] \exp[-\mathbf{R}\tau]^*\bar{\mathbf{a}}(0) = T^{-1} \exp[-\Lambda(\tau + t)]T(T^{-1})^* \exp[-\Lambda\tau]^* T^*\bar{\mathbf{a}}(0) \tag{A15}$$

where T is the matrix which diagonalizes $\mathbf{R}$, and Λ is the diagonal matrix of its eigenvalues, λ_l. Since immediately after the first $(\pi/2)_{-x}$ pulse the magnetization is purely I_y, it follows that $G(\phi,0) = 1$ is independent of ϕ, so that for all $k \neq 0$, $\bar{a}_k(0) = 0$ while $\bar{a}_0(0) = 1$. Substituting in (A15) and using (A7) gives for the FID(t) of a single domain

$$\text{FID}(t) \propto \bar{a}_0(t) = \text{Re}\sum\{(T^{-1})_{1l} \exp[\lambda_l(\tau + t)](T)_{lk}(T^{-1})^*_{kj} \exp(\lambda_j\tau)^*(T^*)_{j1}\} \tag{A16}$$

(iii) **Comparison of the Planar Jump and Diffusion Spectra.** Although in the fast motion limit both the three-site jumps and the planar diffusion models should yield identical line shapes, in the slow and intermediate regimes they may differ. To check on the sensitivity of the line shape to this effect we compare in Figure 14 simulated powder spectra calculated on the basis of the two models. They are arranged pairwise so as to resemble each other as much as possible within each couple. Although very small differences may be seen, these are usually too insignificant to be observed experimentally. We therefore feel that by line-shape analysis alone it would be difficult to distinguish between the two mechanisms. For the particular parameters used for the calculations in Figure 14, it may be seen that pairwise matching of spectra is obtained for $(1/\tau_J)/D_R \approx 2.7$ to 3.0, so that if one prefers to interpret the spectra in the main text in terms of a three-site jump model, the ordinate in Figure 3 must be scaled accordingly.

We have also compared the dependence of the line shape on the time interval, τ, between the $\pi/2$ pulses, for the two dynamic models. Although the line shapes were indeed quite sensitive to τ, as discussed in the main text, the dependence on this parameter seemed to be very similar for both mechanisms.

Registry No. I-8, 96189-55-8; I-9, 96189-56-9; I-10, 96189-57-0; II-13, 96189-66-1.